*Acta Cryst.* (1990). B46, 577–586

# Charge Density in $(NH_4)_2Cr(SO_4)_2.6H_2O$ at 84 K: a Jahn–Teller Distorted Complex

BY BRIAN N. FIGGIS,* EDWARD S. KUCHARSKI AND PHILIP A. REYNOLDS

*School of Chemistry, University of Western Australia, Nedlands, Western Australia* 6009, *Australia*

(*Received* 3 *October* 1989; *accepted* 16 *May* 1990)

## Abstract

Diammonium hexaaquachromium(II) disulfate, $[NH_4]_2[Cr(H_2O)_6](SO_4)_2$, $M_r = 388{\cdot}29$. At 84 (2) K, the structure is monoclinic, $P2_1/a$, $a = 9{\cdot}490$ (2), $b = 12{\cdot}816$ (3), $c = 6{\cdot}104$ (1) Å, $\beta = 107{\cdot}09$ (2)°, $V = 710$ (1) Å$^3$, $Z = 2$, $D_x = 1{\cdot}82$ Mg m$^{-3}$, $\lambda$(Mo $K\alpha$) = 0·71069 Å, $\mu = 1{\cdot}196$ mm$^{-1}$, $F(000) = 405{\cdot}2$, $R(I) = 0{\cdot}022$, $R(F) = 0{\cdot}030$ for 7490 reflections. The $CrO_6$ octahedron has a large Jahn–Teller distortion with a tetragonal elongation of Cr—O(8) 2·389 (1) Å; Cr—O(7) 2·079 (1), Cr—O(9) 2·053 (1) Å. At 295 (2) K, the structure is monoclinic, $P2_1/a$, $a = 9{\cdot}424$ (2), $b = 12{\cdot}699$ (3), $c = 6{\cdot}204$ (1) Å, $\beta = 106{\cdot}60$ (1)°, $V = 712$ (1) Å$^3$, $Z = 2$, $D_m = 1{\cdot}80$ (1), $D_x = 1{\cdot}81$ Mg m$^{-3}$, $\lambda$(Mo $K\alpha$) = 0·71069 Å, $\mu = 1{\cdot}199$ mm$^{-1}$, $F(000) = 405{\cdot}2$, $R(I) = 0{\cdot}020$, $R(F) = 0{\cdot}024$ for 4339 reflections. The $CrO_6$ octahedron has a slightly smaller Jahn–Teller distortion with tetragonal elongation Cr—O(8) 2·323 (2) Å; Cr—O(7) 2·125 (2), Cr—O(9) 2·054 (1) Å. The $CrO_6$ geometry has an unusual temperature dependence. The valence-orbital populations from the refinement give, in the $Cr(OH_2)_6$ unit, Cr-atom populations of $3d_{xy}^{1.26\,(3)}\,3d_{xz,yz}^{2.04\,(4)}\,3d_{z^2}^{0.88\,(4)}\,3d_{x^2-y^2}^{0.28\,(3)}\,4p_{x,y}^{-0.32\,(16)}\,4p_z^{0.39\,(15)}$, which show the substantial differences expected on the grounds of the large Jahn–Teller effect present. The two short Cr—O bonds show much greater covalent charge transfer from the O lone pairs to the Cr atom than does the longer bond. For the shorter bonds distinct accummulation of charge in the mid-bond region is observed. The populations within the ammonium and sulfate ions present the expected features and preserve ideal tetrahedral symmetry accurately, and the charge distributions within them are unremarkable. The ionic charges depart from the ideal values, apparently owing to charge transfers associated with the strong hydrogen bonding in the crystal. They are, approximately, $[Cr(OH_2)_6]^{1.2+}$, $[SO_4]^{1.5-}$ and $[NH_4]^{0.9+}$, with some variation according to the method of analysis, as expected.

## Introduction

The title compound is the only one of the eight known ammonium Tutton salts of the first transition series whose structure has not yet been determined. It has been prepared in powder form by Earnshaw, Larkworthy, Patel & Beech (1969), and preliminary studies by ESR (Abragam & Pryce, 1951) and by spectroscopy (Earnshaw *et al.*, 1969) have been carried out. No other experiments seem to have been reported, which contrasts with the wealth of data on the other members of the series.

The other seven compounds have all been studied. Initial studies were by X-ray diffraction film methods (Grimes, Kay & Webb, 1963; Montgomery & Lingafelter, 1964*a*,*b*, 1966; Webb, Kay & Grimes, 1965; Montgomery, Chastain & Lingafelter, 1966; Montgomery, Chastain, Natt, Witkowska & Lingafelter, 1967). These were followed by more accurate X-ray diffractometer studies for the copper (Alcock, Duggan, Murray, Tyagi, Hathaway & Hewat, 1984; Maslen, Ridout & Watson, 1988) and nickel (Treushnikov, Kuskov, Soboleva & Belov, 1978; Maslen, Ridout, Watson & Moore, 1988) isomorphs, and by single-crystal neutron diffraction studies at room temperature for the copper (Brown & Chidambaram, 1969; Maslen, Watson & Moore, 1988) and nickel (Maslen, Ridout, Watson & Moore, 1988) salts. Neutron diffraction determinations were also performed at 4·2 K for the deuterated vanadium (Deeth, Figgis, Forsyth, Kucharski & Reynolds, 1989), hydrogenous manganese (Fender, Figgis, Forsyth, Reynolds & Stevens, 1986), deuterated iron (Figgis, Kucharski, Reynolds & Tasset, 1989), and both hydrogenous and deuterated nickel (Fender, Figgis & Forsyth, 1986*a*) compounds; a study of the deuterated copper salt by powder neutron diffraction between 5 and 295 K is reported in Hathaway & Hewat (1984).

Much of the later work has been concerned with charge-density (Treushnikov *et al.*, 1978; Maslen, Ridout & Watson, 1988; Maslen, Ridout, Watson & Moore, 1988; Maslen, Watson & Moore, 1988) and spin-density (Fender, Figgis, Forsyth, Reynolds & Stevens, 1986; Fender, Figgis & Forsyth, 1986*b*; Figgis, Forsyth, Kucharski, Reynolds & Tasset, 1989) diffraction studies to elucidate bonding in the metal hexaaqua ions. The present study of the chromium(II) compound has also been carried out in connection with charge density and spin density; we plan to examine spin density later.

* To whom correspondence should be addressed.

0108-7681/90/050577-10$03.00

A complication concerning the cation in the $Cu^{II}$ salt has been investigated by Alcock *et al.* (1984), Hathaway & Hewat (1984) and Riley, Hitchman & Mohammed (1987). There are unusual Cu—O bond-length changes, and probably an impending phase transition associated with large librational motion of the perdeuteroammonium ions, possibly involving disorder. Any nuclear disorder is obviously undesirable in a charge-density study. Accordingly, we have collected data at two temperatures for the $Cr^{II}$ salt, where similar Jahn–Teller effects may operate.

Spin densities can be measured more precisely than can charge densities, although the amount of polarized neutron diffraction data which can be obtained is much more limited than for X-ray studies. Recently our group has measured the spin densities in the hexaaquametal ions of $V^{II}$, $Mn^{II}$, $Fe^{II}$, and $Ni^{II}$ contained in the ammonium Tutton salts (Fender, Figgis, Forsyth, Reynolds & Stevens, 1986; Fender, Figgis & Forsyth, 1986*b*; Deeth *et al.*, 1989; Figgis, Forsyth *et al.*, 1989). The results obtained clearly show the effects of covalence.

Three charge-density experiments have been performed on cobalt(III)–ammine hexacyanochromium salts which, when analysed, also show covalence effects (Iwata, 1977; Figgis, Reynolds & Wright, 1983; Figgis & Reynolds, 1985). Recently, charge-density studies at 295 K have been published for the Cu, Ni and Mg ammonium Tutton salts (Maslen, Ridout & Watson, 1988; Maslen, Watson & Moore, 1988), which show interesting qualitative effects, and there is a study at 295 K of the salt chromium(II) sulfate pentahydrate (Vaalsta & Maslen, 1987).

We present here a charge-density study of the ammonium $Cr^{II}$ Tutton salt. The crystal contains ammonium, sulfate and hexaaquachromium(II) ions. The object of the experiment is to study the Jahn–Teller-distorted $[Cr(OH_2)_6]^{2+}$ ion. This shows two distinctly different metal–water bond lengths. By comparison of the two water types and the Cr-atom electron configuration we demonstrate that charge flows associated with the bonding between the Cr atom and the water molecule are significant and can be measured.

## Experimental

The following operations were performed with the rigorous exclusion of air. Chromium metal (99·999%, United Mineral & Chemical Co.) was treated with warm 3·6 *M* sulfuric acid. After some of the metal had dissolved bright-blue $CrSO_4.5H_2O$ commenced to separate. When most of the chromium had dissolved the solution was heated to dissolve the product and filtered to remove the remaining metal. The filtrate was cooled slowly to 273 K and the crystalline $CrSO_4.5H_2O$ filtered off, washed with a small amount of aqueous alcohol, and dried *in vacuo*. This material is stable in dry air. $CrSO_4.5H_2O$ (1·0 g) was dissolved in warm water (3·0 ml) containing $(NH_4)_2SO_4$ (1·5 g). On cooling and allowing the solution to stand small blue crystals of ammonium chromous Tutton salt appeared, a few well formed. They were washed with aqueous alcohol and rapidly dried *in vacuo*. This material is stable in dry air for a limited time. Analysis: found Cr 13.39 (6), S 16.45 (8)%; calculated Cr 13.39, S 16.51%.

A crystal, which had dimensions 0·215 (010 and $0\bar{1}0$), 0·129 ($20\bar{1}$ and $\bar{2}01$), 0·218 ($\bar{2}1\bar{3}$), 0·158 (100), 0·187 mm (302) from an arbitrary centre, was mounted on a Syntex $P2_1$ diffractometer with a locally developed low-temperature nitrogen-gas-flow accessory operating at 84 (2) K. Graphite-monochromatized Mo $K\alpha$ radiation was employed. The unit cell was determined by the least-squares fitting of the setting angles of 14 well-spaced reflections with $35 < 2\theta < 39°$. A complete sphere of data was collected to $2\theta = 100°$. An $\omega$–$2\theta$ scan was employed. A second sphere, to 60°, was also collected. In all, 30 393 reflections were measured. The six standards, measured after each 94 reflections, showed no significant change in intensity over the data-collection period. 4458 reflections with $I/\sigma(I) > 30\sigma$ and $I < 200\,000$ counts (maximum count for any reflection 2 500 000) were used to refine the crystal dimensions to maximize the agreement between equivalent reflections (Figgis, Kucharski & Reynolds, 1989). An analytical absorption correction was then carried out; the transmission factor varied from 0·754 to 0·636. These corrected data were reduced by averaging equivalents to give 7490 unique reflections, with $(\sin\theta/\lambda)_{max} = 1{\cdot}08$ Å$^{-1}$, $|h| < 14$, $|k| < 18$, $|l| < 9$. $R_{int} = 0{\cdot}022$.

A second crystal, of dimensions 0·190 (010 and $0\bar{1}0$), 0·102 ($20\bar{1}$ and $\bar{2}01$), 0·159 mm (101 and $\bar{1}0\bar{1}$) from an arbitrary centre, was coated with a thin layer of araldite. At 295 (2) K a new cell was determined and spheres of data collected under the same conditions as above. 34 355 reflections were measured, giving, after absorption correction as before (transmission 0·793–0·683), $R_{int} = 0{\cdot}040$. The data of the wavevector, $|\mathbf{k}|$, $> 0{\cdot}9$ Å$^{-1}$ were very weak [86% $I < 3\sigma(I)$], and so were omitted from further refinements, leaving 4339 unique data.

## Initial density refinements

Starting with the parameters of the $V^{II}$ structure (Deeth *et al.*, 1989), refinement was carried out using the program *ASRED* (Figgis, Reynolds & Williams, 1980). Scattering factors for non-H-atom valence and core functions were calculated using the program *JCALC* (Figgis, Reynolds & White, 1987) from

Table 1. *Results of various refinements*

Y/N indicates that a parameter set was/was not refined.

| | Type of refinement | | | | | |
|---|---|---|---|---|---|---|
| | Spherical theoretical | Spherical valence | | Aspherical | | Symmetry constrained |
| | R1 | R2 | R3 | R4 | R5 | R6 |
| NVP[a] | 0 | 21 | 21 | 89 | 89 | 36 |
| $P_{core}$[b] | N | N | N | Y | N | N |
| $a_{iso}$[c] | N | N | N | N | Y | Y |
| $F(000)$ | 405·2 | 405·2 | 414·5 | 428·1 | 428·1 | 427·2 |
| Scale | 9·27 (7) | 9·20 (1) | 9·18 (1) | 9·16 (3) | 9·23 (3) | 9·24 (1) |
| $R(I)$ | 0·047 | 0·037 | 0·037 | 0·021 | 0·021 | 0·022 |
| $wR(I)$ | 0·061 | 0·053 | 0·053 | 0·034 | 0·034 | 0·035 |
| $R(F)$[d] | 0·038 | 0·037 | 0·037 | 0·029 | 0·030 | 0·030 |
| $\chi^2$[e] | 1·78 | 1·56 | 1·55 | 0·99 | 1·00 | 1·02 |

Notes: (*a*) number of valence parameters; (*b*) core populations; (*c*) quartic anharmonic parameters; (*d*) $I > 3\sigma(I)$; (*e*) goodness-of-fit.

the wavefunctions of Clementi & Roetti (1974), and were modified for anomalous dispersion (Cromer & Liberman, 1970). The hydrogen-scattering functions were taken from Stewart, Davidson & Simpson (1965). All 7490 reflections to a maximum wavevector of 1·08 Å$^{-1}$ were used and the function $\sum[\sigma(I)]^{-2}/[I(\text{obs.}) - I(\text{calc.})]^2$ was minimized until a maximum shift/e.s.d. of 0·1 was obtained. A type-I extinction parameter, together with another proportional to $I^2$, and an angle-independent multiple-scattering parameter were used as for $Cs_3CoCl_5$ (Figgis, Kucharski & Reynolds, 1989). Positional and anisotropic thermal parameters were refined (isotropic for H atoms). We modelled the valence density by sets of multipolar density functions, closely following our previous procedure (Figgis *et al.*, 1987; Figgis, Kucharski & Reynolds, 1989). As an initial benchmark we refined a conventional model of spherical theoretical neutral atomic functions to describe the charge density, giving refinement R1, the results of which are shown in Table 1.

The charge-density models were constructed with the minimum set of chemically reasonable valence orbitals. There were five 3*d* and three 4*p* orbitals on Cr, four ($sp^3$) hybrid orbitals on S, N and water O(7)—O(9), two $2p_\pi$ and two (*sp*) hybrid orbitals on sulfate O(3)—O(6), and 1*s* orbitals on the H-atom sites. The low site symmetries present in the crystal would necessitate many more multipoles to obtain similar highest-order functions – 101 variables *versus* the 51 here.

The axis system points at neighbouring atoms: Cr, $z \rightarrow$O(8), $x \rightarrow$O(7); S, $z$ in the O(3)–O(4)–S plane, $x \rightarrow$O(4); O(3) to O(6), $x \rightarrow$S; O(7) to O(9), $x \rightarrow$Cr, $z$ in the plane defined by Cr—O and the mid-point of attached H atoms; N, $x \rightarrow$H(11), $z$ in the N–H(11)–H(12) plane. Examination of difference maps showed large peaks in the middle of the sulfate S—O bonds. Accordingly, Gaussian functions of mean-square width 0·16 Å$^2$ were placed there [$X(3)$–$X(6)$], and similar functions [$X(7)$–$X(9)$] were placed at the mid-point of the three Cr—O bonds. $X(3)$–$X(6)$ turn out to have relatively large populations, so we were also able to refine their positions and widths as well as their populations. In addition, all heavy-atom valence-function radii were allowed to vary in the manner of the usual '$\kappa$' refinement. For the (*sp*) hybrids $(sp)_1$ points along $+x$, $(sp)_2$ along $-x$, $(sp^3)_1$ along $+x$, and $(sp^3)_2$ lies in the $xz$ plane.

### Anharmonicity *versus* variable core densities

On fixing the Gaussian-function populations [$X(3)$—$X(9)$] at zero and constraining the atom fragments to be spherical we obtained the refinement result R2. We knew from the earlier study on $Cs_3CoCl_5$ (Figgis, Kucharski & Reynolds, 1989) that these atom-centred charge models are not adequate and that significant diffuse-density changes connected with intermolecular, crystal-based, effects occur. A simple way to improve the model is to assume these give a uniform density distribution, so we removed the constraint on $F(000)$, which forces electroneutrality, to give refinement R3. The scale factor was then obtained from the contribution of the fixed-core populations to the scattering. Traditionally, this is achieved by refinement of the high-angle data alone. When we refined high-angle and low-angle data separately we obtained very different scale factors, separated by some by 5%, and a corresponding variation in the thermal parameters, which were somewhat correlated.

When we allowed the light-atom core populations to vary, keeping only the Cr core fixed, and with $F(000)$ unconstrained, giving refinement R4, the fit improved dramatically. The C and N core populations decreased from 2·00 to about 1·7 e, but that of S was not significantly changed. As an alternative procedure, we introduced an isotropic quartic thermal parameter for each non-H atom, keeping the core populations fixed, and we obtained refinement R5. The resulting anharmonic parameters are significant and depress scattering at higher wavevectors. Thus we had an empirical observation; decreasing *or* anharmonically smearing light-atom core electrons improved our scattering model. Other work suggested that the effect is genuine anharmonicity, and unconnected with core-electron changes. We discuss the core-population changes first.

In all-light-atom structures, if the core populations indeed vary, several effects produced by the assumption of fixed cores should be obvious. The incorrect scale would produce only a small core-deformation density, instead of the 'true' hole. The thermal parameters derived by fitting X-ray data would be lower than those from neutron diffraction or calculated from phonon-dispersion curves. This latter

effect has already been seen in diamond by Stewart (1973). The use of neutron diffraction fixes positional and thermal parameters, but the scale still comes entirely from X-ray diffraction. Thus any discrepancy is observed only indirectly in the comparison of thermal parameters derived separately from X-ray and neutron diffraction. Given the large and different effects of thermal-diffuse scattering on each of these experiments, it would be difficult to derive an appropriate scale.

Theoretical calculations provide two sources for core-population reductions. Firstly, as Stewart points out, free-atom calculations of the quality of Clementi & Roetti (1974) are not exact. For example they do not satisfy the rigorous cusp-constraint condition. Stewart remedied this in a slightly arbitrary way, and produced agreement between X-ray and neutron experiments by effectively reducing the core density in diamond by almost 5%. Secondly, changes occur in core bonding on molecule formation. Good-quality Hartree–Fock limit calculations on diatomics almost always show a hole in the core region in density maps. Integration of this data in several cases (B. N. Figgis, unpublished results) shows a core reduction of *ca* 0·05 e.

To investigate this point further we have recently examined (Reynolds & Figgis, 1989) the extensive and very accurate structure factors of silicon obtained by interferometry, now available in the literature. We conclude that a small core-population reduction of *ca* 0·05 e and the introduction of an isotropic quartic thermal parameter are both necessary and adequate to explain the data. Non-rigid silicon pseudoatoms are not necessary, though we cannot exclude the possibility.

In the present example we see that core reduction of *ca* 0·3 e is not supported, but that substantial quartic anharmonic terms are. However, whatever the explanation of the difference between the high- and low-angle scale factors, because they provide a better and more consistent fit, and thus a more reliable dissection of the total scattering into atom-density fragments, we use quartic isotropic anharmonic thermal parameters in this study.

### Final electron density refinements

Our initial anharmonic valence-density refinement (R5) uses all data and optimizes the positional, thermal and valence parameters specified in the previous section. For the 295 K data, because they do not extend as far in reciprocal space as those at 84 K, unacceptable correlations between valence and thermal-motion parameters appeared. These were removed by fixing the valence-function radial parameters and overlap form-factor parameters at the values obtained at 84 K and making the S- and N-atom valence parameters isotropic. This illustrates that, even for this simple, minimal, valence model at 295 K, thermal and valence effects cannot be disentangled. However, at 84 K the greater extent of the data in the wavevector does allow such a separation.

Table 2. *Atomic fractional positional coordinates* ($\times 10^4$, *except for* H, $\times 10^3$ *at* 295 K; $\times 10^5$, *except* H, $\times 10^3$ *at* 84 K), *equivalent isotropic thermal parameters* (Å$^2$ $\times 10^3$ *at* 295 K, Å$^2$ $\times 10^4$ *at* 84 K) *and quartic anharmonic parameter* $\gamma$ (Å$^4$)

$U_{eq} = \frac{1}{3}(U_{11} + U_{22} + U_{33})$. $\gamma$ is defined by the thermal factor $T = \exp[-2\pi^2(h^2a^{*2}U_{11} + \cdots + 2hka^*b^*U_{12} + \cdots)](1 - \gamma|\mathbf{k}|^4)$.

| | $x$ | $y$ | $z$ | $U_{eq}$ | $\gamma$ |
|---|---|---|---|---|---|
| (*a*) 295 K | | | | | |
| Cr | 0 | 0 | 0 | 22 | 0·10 (3) |
| S | 3965 (1) | 1412 (1) | 7426 (1) | 26 | 0·26 (5) |
| O(3) | 3920 (2) | 2348 (1) | 5971 (2) | 44 | 0·57 (11) |
| O(4) | 5365 (2) | 846 (1) | 7723 (1) | 50 | 0·73 (12) |
| O(5) | 2726 (2) | 707 (1) | 6279 (2) | 35 | 0·44 (9) |
| O(6) | 3800 (1) | 1741 (1) | 9627 (3) | 40 | 0·53 (12) |
| O(7) | 1677 (2) | 1071 (1) | 1713 (2) | 43 | 0·48 (11) |
| O(8) | −1802 (2) | 1170 (1) | 402 (3) | 41 | 0·21 (11) |
| O(9) | −10 (1) | −713 (1) | 2967 (2) | 31 | 0·17 (7) |
| N | 1271 (1) | 3560 (1) | 3643 (2) | 42 | 0·78 (19) |
| H(11) | 69 (2) | 345 (1) | 252 (3) | 55 | |
| H(12) | 189 (2) | 316 (1) | 393 (2) | 52 | |
| H(13) | 91 (2) | 357 (1) | 460 (3) | 74 | |
| H(14) | 162 (2) | 412 (2) | 360 (2) | 62 | |
| H(15) | 211 (2) | 95 (1) | 313 (4) | 31 | |
| H(16) | 237 (2) | 127 (1) | 119 (3) | 25 | |
| H(17) | −263 (2) | 106 (1) | −39 (2) | 27 | |
| H(18) | −157 (2) | 178 (2) | 15 (2) | 28 | |
| H(19) | −82 (2) | −66 (1) | 326 (2) | 16 | |
| H(20) | 30 (2) | −135 (1) | 323 (2) | 14 | |
| (*b*) 84 K | | | | | |
| Cr | 0 | 0 | 0 | 72 | 0·01 (1) |
| S | 38917 (1) | 14293 (1) | 74827 (2) | 73 | 0·03 (1) |
| O(3) | 37872 (3) | 23646 (3) | 60319 (6) | 142 | 0·24 (3) |
| O(4) | 52962 (5) | 08894 (3) | 77213 (5) | 148 | 0·19 (2) |
| O(5) | 26572 (4) | 07175 (3) | 63351 (5) | 118 | 0·15 (2) |
| O(6) | 37705 (3) | 17253 (2) | 97681 (6) | 136 | 0·22 (2) |
| O(7) | 16291 (5) | 10439 (3) | 17135 (5) | 144 | 0·15 (2) |
| O(8) | −18323 (4) | 11776 (3) | 5005 (7) | 157 | 0·27 (3) |
| O(9) | 664 (4) | −7196 (3) | 30340 (6) | 125 | 0·18 (2) |
| N | 12691 (5) | 36404 (3) | 37701 (6) | 154 | 0·35 (3) |
| H(11) | 59 (1) | 351 (1) | 260 (2) | 230 | |
| H(12) | 189 (1) | 317 (1) | 412 (1) | 269 | |
| H(13) | 93 (1) | 373 (1) | 481 (2) | 254 | |
| H(14) | 167 (1) | 418 (1) | 357 (1) | 307 | |
| H(15) | 200 (1) | 93 (1) | 315 (2) | 115 | |
| H(16) | 230 (1) | 120 (1) | 117 (1) | 52 | |
| H(17) | −266 (1) | 109 (1) | −34 (1) | 139 | |
| H(18) | −164 (1) | 178 (1) | 29 (1) | 84 | |
| H(19) | −72 (1) | −70 (1) | 337 (1) | 81 | |
| H(20) | 32 (1) | −135 (1) | 322 (1) | 25 | |

The atomic coordinates and equivalent isotropic thermal parameters which resulted from the above refinements are given in Table 2. The principal interatomic distances and angles, obtained using the *XTAL* system (Hall & Stewart, 1989), are given in Table 3.* Selected valence-density results are given in Table 4.

* Lists of least-squares planes for the $Cr(OH_2)_6^{2+}$ cation, anisotropic thermal parameters, valence-density results, and $F$(obs.) and $F$(calc.) for both temperatures have been deposited with the British Library Document Supply Centre as Supplementary Publication No. SUP 53115 (23 pp.). Copies may be obtained through The Technical Editor, International Union of Crystallography, 5 Abbey Square, Chester CH1 2HU, England.

Table 3. *Bond lengths* (Å) *and angles* (°)

| | 295 K | 84 K |
|---|---|---|
| Directly bonded atoms | | |
| Cr—O(7) | 2·125 (2) | 2·0792 (5) |
| Cr—O(8) | 2·323 (2) | 2·3889 (5) |
| Cr—O(9) | 2·054 (1) | 2·0532 (5) |
| O(7)—H(15) | 0·87 (2) | 0·86 (1) |
| O(7)—H(16) | 0·85 (2) | 0·82 (1) |
| O(8)—H(17) | 0·80 (2) | 0·81 (1) |
| O(8)—H(18) | 0·83 (2) | 0·82 (1) |
| O(9)—H(19) | 0·84 (2) | 0·83 (1) |
| O(9)—H(20) | 0·86 (2) | 0·84 (1) |
| S—O(3) | 1·486 (1) | 1·4762 (5) |
| S—O(4) | 1·467 (2) | 1·4705 (5) |
| S—O(5) | 1·482 (1) | 1·4875 (4) |
| S—O(6) | 1·478 (2) | 1·4824 (5) |
| N—H(11) | 0·77 (2) | 0·83 (1) |
| N—H(12) | 0·76 (2) | 0·83 (1) |
| N—H(13) | 0·77 (2) | 0·80 (1) |
| N—H(14) | 0·79 (2) | 0·82 (1) |
| O(7)—Cr—O(8) | 89·96 (6) | 89·47 (2) |
| O(7)—Cr—O(9) | 91·56 (5) | 90·81 (2) |
| O(8)—Cr—O(9) | 90·28 (5) | 90·07 (2) |
| Cr—O(7)—H(15) | 117·5 (10) | 115·1 (5) |
| Cr—O(7)—H(16) | 122·7 (11) | 120·0 (6) |
| Cr—O(8)—H(17) | 115·4 (12) | 115·8 (6) |
| Cr—O(8)—H(18) | 109·6 (12) | 112·3 (6) |
| Cr—O(9)—H(19) | 113·4 (8) | 114·8 (6) |
| Cr—O(9)—H(20) | 119·6 (10) | 118·8 (6) |
| H(15)—O(7)—H(16) | 104·7 (17) | 108·9 (8) |
| H(17)—O(8)—H(18) | 108·1 (13) | 104·8 (7) |
| H(19)—O(9)—H(20) | 108·5 (15) | 104·2 (9) |
| O(3)—S—O(4) | 109·68 (9) | 109·91 (2) |
| O(3)—S—O(5) | 108·04 (7) | 108·11 (2) |
| O(3)—S—O(6) | 110·05 (7) | 110·28 (2) |
| O(4)—S—O(5) | 108·72 (8) | 108·87 (3) |
| O(4)—S—O(6) | 110·53 (5) | 110·25 (2) |
| O(5)—S—O(6) | 109·78 (7) | 109·38 (2) |
| H(11)—N—H(12) | 112·6 (15) | 113·1 (7) |
| H(11)—N—H(13) | 110·3 (20) | 108·6 (9) |
| H(11)—N—H(14) | 109·5 (14) | 109·1 (7) |
| H(12)—N—H(13) | 107·8 (15) | 108·8 (8) |
| H(12)—N—H(14) | 109·0 (18) | 108·8 (9) |
| H(13)—N—H(14) | 107·4 (14) | 108·4 (8) |
| Hydrogen bonds | | |
| H(15)—O(5) | 1·90 (2) | 1·88 (1) |
| H(16)—O(6) | 1·97 (2) | 1·96 (1) |
| H(17)—O(4) | 1·94 (2) | 1·96 (1) |
| H(18)—O(6) | 1·96 (2) | 2·00 (1) |
| H(19)—O(5) | 1·90 (2) | 1·90 (1) |
| H(20)—O(3) | 1·82 (2) | 1·84 (1) |
| H(11)—O(6) | 2·15 (2) | 2·08 (1) |
| H(12)—O(3) | 2·22 (2) | 2·10 (1) |
| H(13)—O(4) | 2·27 (2) | 2·10 (1) |
| H(14)—O(5) | 2·10 (2) | 2·07 (1) |
| O(7)—H(15)—O(5) | 170·6 (19) | 175·0 (9) |
| O(7)—H(16)—O(6) | 173·4 (15) | 173·5 (9) |
| O(8)—H(17)—O(4) | 177·6 (15) | 177·6 (10) |
| O(8)—H(18)—O(6) | 174·3 (17) | 178·7 (9) |
| O(9)—H(19)—O(5) | 172·5 (12) | 170·9 (8) |
| O(9)—H(20)—O(3) | 174·2 (12) | 169·3 (8) |
| N—H(11)—O(6) | 170·1 (20) | 174·7 (9) |
| N—H(12)—O(3) | 157·6 (13) | 158·8 (7) |
| N—H(13)—O(4) | 157·9 (13) | 171·7 (7) |
| N—H(14)—O(5) | 170·6 (16) | 163·0 (9) |

Deformation density and residual density maps based on refinement R5 were constructed using the scale, thermal and positional parameters to obtain experimental structure factors, from which were subtracted theoretical spherical and the fitted structure factors respectively. The maps are shown in Figs. 1–10 for three metal hexaaqua ion planes, and a representative sulfate and ammonium ion plane. A wavevector cutoff of 0·8 $Å^{-1}$ was used. Away from the atomic cores, the uncertainty resulting from random structure-factor errors is less than

Table 4. *Selected valence parameters obtained from the constrained refinement R6, rescaled to formula number of electrons*

| | Valence parameters | | | | |
|---|---|---|---|---|---|
| Cr | $3d_{xy}$ 1·26 (3) | $3d_{xz}$ 1·02 (2) | $3d_{yz}$ $= 3d_{xz}$ | $3d_{x^2-y^2}$ 0·28 (3) | $3d_{z^2}$ 0·88 (4) |
| | $4p_x$ −0·16 (8) | $4p_y$ $= 4p_x$ | $4p_z$ 0·39 (15) | $r_{3d}$ 0·97 (1) | |
| S | $(sp^3)_1$ 0·70 (2) | $(sp^3)_2$ $= (sp^3)_1$ | $(sp^3)_3$ $= (sp^3)_1$ | $(sp^3)_4$ $= (sp^3)_1$ | $r_{3sp}$ 0·94 (1) |
| O(3), O(4), O(5), O(6) | $2p_\pi$ 3·58 (2) | $(sp^1)_1$ 1·38 (2) | $(sp^1)_2$ 1·55 (1) | $r_{2sp}$ 1·042 (3) | |
| O(7), O(9) | $(sp^3)_1$ 1·74 (2) | $(sp^3)_2$ 1·63 (2) | $(sp^3)_3$ 1·63 (1) | $(sp^3)_4$ $= (sp^3)_3$ | $r_{2sp}$ 1·046 (4) |
| O(8) | $(sp^3)_1$ 1·84 (2) | $(sp^3)_2$ 1·50 (3) | $(sp^3)_3$ 1·60 (2) | $(sp^3)_4$ $= (sp^3)_3$ | $r_{2sp}$ 1·033 (6) |
| N | $(sp^3)_1$ 1·01 (4) | $(sp^3)_2$ $= (sp^3)_1$ | $(sp^3)_3$ $= (sp^3)_1$ | $(sp^3)_4$ $= (sp^3)_1$ | $r_{2sp}$ 0·89 (2) |
| | 1s | | | 1s | |
| H(11)–H(14) | 1·06 (4) | | H(17), H(18) | 0·76 (2) | |
| H(15), H(16) | 0·65 (1) | | H(19), H(20) | 0·65 (1) | |
| | $z[X(6)]$ | $U$ (Å$^2$) | Population | | |
| $X(3)$–$X(6)$ | 0·859 (2) | 0·120 (2) | 0·63 (2) | | |
| $X(7)$, $X(9)$ | | | 0·15 (2) | | |
| $X(8)$ | | | 0·00 (2) | | |

0·05 e $Å^{-3}$. This is less than other systematic errors and is not further discussed.

Examination of the valence-refinement results shows that the valence-electron density is little different from that of a more highly constrained symmetric model. We constrained the $Cr(OH_2)_6$ fragment to pseudo-tetragonal symmetry. We set the $X(7)$–O(7)–H(15)–H(16) parameters equal to the $X(9)$–O(9)–H(19)–H(20) parameters, and in addition made the H-atom populations on each individual water molecule the same. On the Cr atom we put the

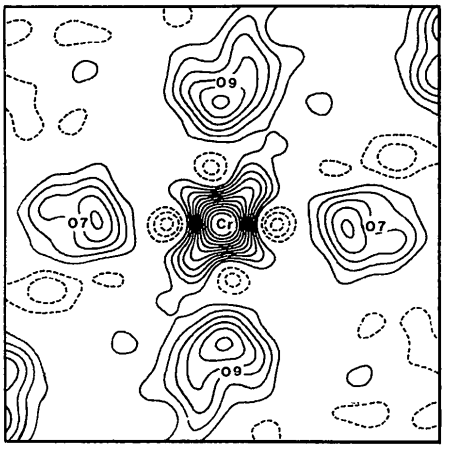


Fig. 1. Deformation density in the $Cr(OH_2)_6$ fragment in the Cr–O(7)–O(9) plane. Contour interval 0·1 e $Å^{-3}$: positive contours solid, negative dotted, zero suppressed. Box size 5·98 × 5·98 Å.

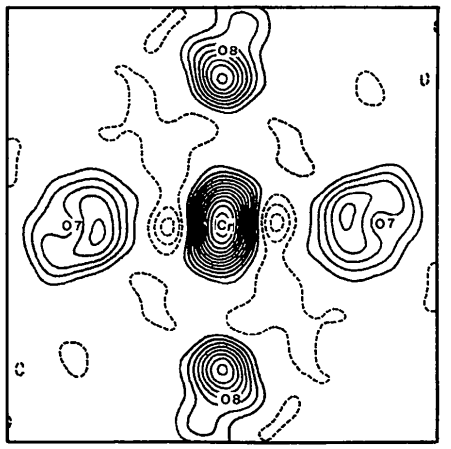


Fig. 2. Deformation density in the $Cr(OH_2)_6$ fragment in the Cr–O(7)–O(8) plane. Details as for Fig. 1.

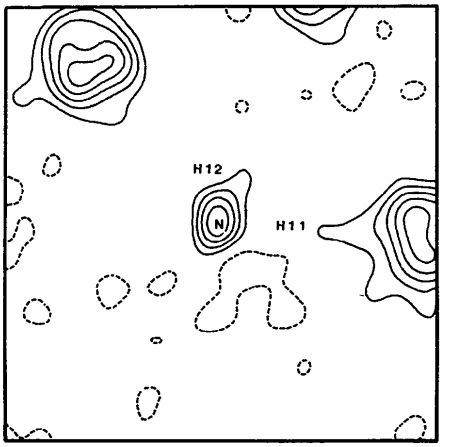


Fig. 5. Deformation density in the $NH_4$ fragment in the N–H(11)–H(12) plane. Details as for Fig. 1.

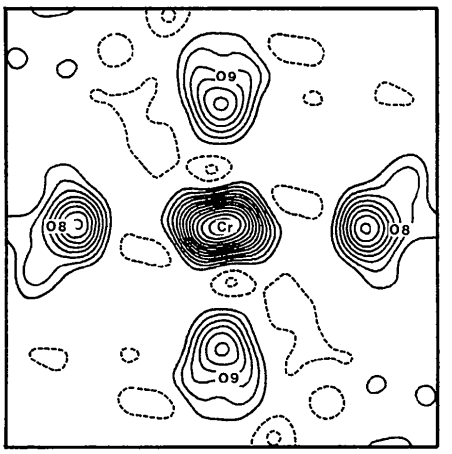


Fig. 3. Deformation density in the $Cr(OH_2)_6$ fragment in the Cr–O(8)–O(9) plane. Details as for Fig. 1.

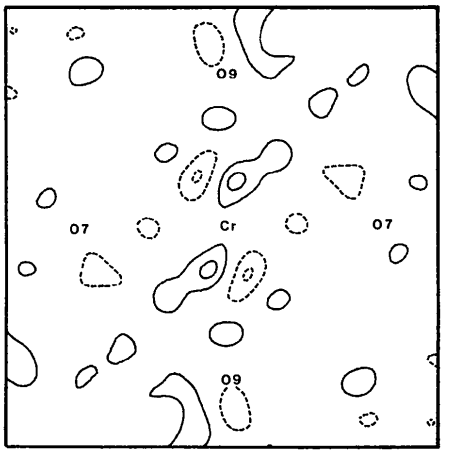


Fig. 6. Residual density in the $Cr(OH_2)_6$ fragment in the Cr–O(7)–O(9) plane. Details as for Fig. 1.

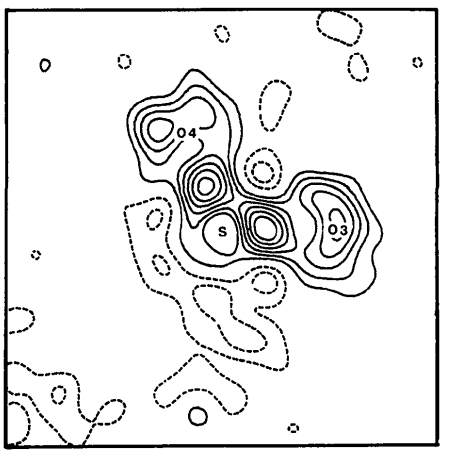


Fig. 4. Deformation density in the $SO_4$ fragment in the S–O(3)–O(4) plane. Details as for Fig. 1.

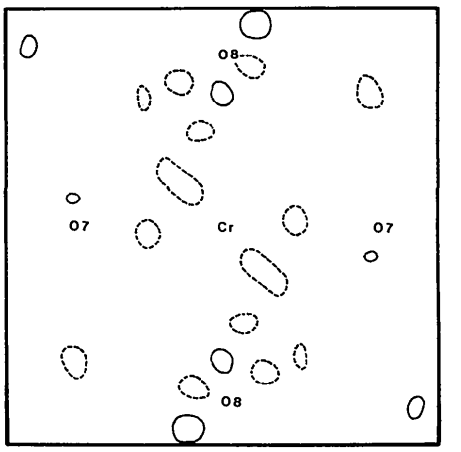


Fig. 7. Residual density in the $Cr(OH_2)_6$ fragment in the Cr–O(7)–O(8) plane. Details as for Fig. 1.

populations $3d_{xz} = 3d_{yz}$ and $4p_x = 4p_y$. On the sulfate ion we imposed tetrahedral symmetry and constrained the Gaussian-function position to vary only along the S—O direction. The ammonium ion we constrained to tetrahedral-valence symmetry. This is refinement R6, and the results are shown in Table 4. The corresponding atom charges are shown in Table 5, where we rescaled the electron count to the theoretical value from the value extrapolated from R6, 427·2, and divided overlap populations equally between the bonded atoms in order to mimic as far as possible the Mulliken population-analysis scheme of theoretical chemistry. The reasons for using this procedure, rather than the equally biasing and arbitrary constraint of electroneutrality, is discussed elsewhere (Figgis, Kucharski & Reynolds, 1989; Figgis *et al.*, 1983). The results of refinements R5 were used, after Fourier transformation of all data of wavevector < 0·8 Å$^{-1}$, to estimate atomic charges by the method of Hirshfeld (1977), using *XTAL*.

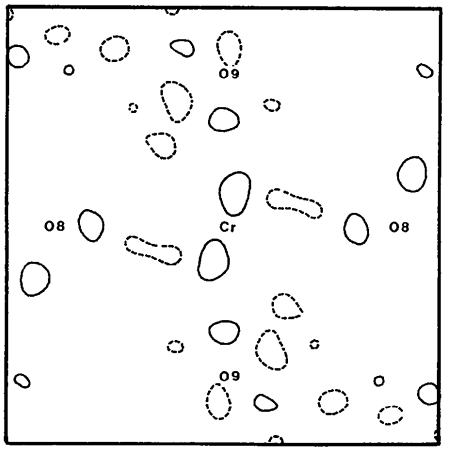


Fig. 8. Residual density in the $Cr(OH_2)_6$ fragment in the Cr–O(8)–O(9) plane. Details as for Fig. 1.

Table 5. *Charges obtained from the refinement R6, rescaled to neutral crystal, and those obtained directly by Fourier methods*

| | Refinement | Fourier |
|---|---|---|
| Cr 3*d* population | 4·45 (7) | — |
| 4*p* population | 0·07 (21) | — |
| Total charge | 1·19 (22) | 0·02 (3) |
| O(7), O(9) | −0·71 (3) | −0·20 (2), 0·22 (2) |
| O(8) | −0·47 (4) | −0·14 (2) |
| H(15), H(16), H(19), H(20) | +0·35 (1) | 0·08 (1), 0·22 (1), 0·22 (1), 0·24 (1) |
| H(17), H(18) | +0·24 (1) | 0·21 (1), 0·18 (1) |
| $O(7)H_2$, $O(9)H_2$ | −0·00 (4) | 0·10 (3), 0·24 (3) |
| $O(8)H_2$ | +0·02 (4) | 0·25 (3) |
| $Cr(OH_2)_6$ | +1·27 (17) | +1·18 (11) |
| S | +1·94 (8) | 0·10 (3) |
| O(3)–O(6) | −0·82 (3) | −0·43 (2), −0·34 (2), −0·48 (2), −0·51 (2) |
| $SO_4$ | −1·33 (13) | −1·66 (5) |
| N | 0·98 (14) | 0·35 (2) |
| H(11)–H(14) | −0·06 (4) | 0·17 (1), 0·19 (1), 0·16 (1), 0·20 (1) |
| $NH_4$ | +0·74 (16) | +1·07 (3) |

## Discussion

### *Hydrogen bonding*

The hydrogen-bond network revealed here differs only in minor ways from that of the other ammonium Tutton salts which have been studied in the past (see *Introduction*). The most substantial difference is in the bonding to H(13). In the other salts studied there is a bifurcated hydrogen bond to O(3) and O(4). Here the relative distances are 2·75 (1) and 2·10 (1) Å, a difference much larger than in the other cases, and effectively the bond is no longer bifurcated. Examination of all sulfate-ion bond lengths and angles, and also hydrogen-bond lengths and angles, compared with the other salts, shows a slightly closer approach to high local symmetry than elsewhere. The sulfate ion is more accurately tetrahedral and the hydrogen bonds more linear (O—H···O) and more equal in length than in any of the other salts studied.

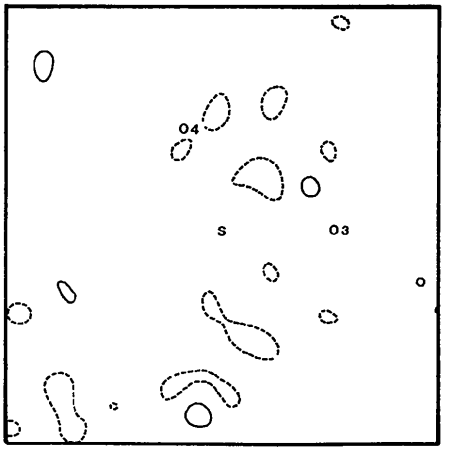


Fig. 9. Residual density in the $SO_4$ fragment in the S–O(3)–O(4) plane. Details as for Fig. 1.

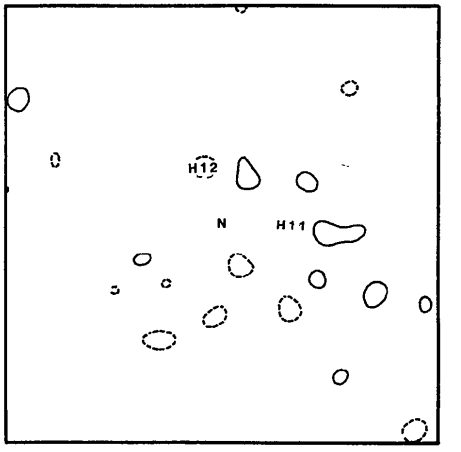


Fig. 10. Residual density in the $NH_4$ fragment in the N–H(11)–H(12) plane. Details as for Fig. 1.

*Jahn–Teller distortion*

The Jahn–Teller distortion of the hexaaqua cation is very large, with a 0·32 Å elongation of Cr—O(8) while Cr—O(7) and Cr—O(9) remain similar. In the hydrogenous copper salt Cu—O(7) is elongated. Hathaway & Hewat (1984) note that in the deuterated copper salt Cu—O(8) is lengthened, in contrast to the hydrogenous copper result. Which bond lengthens obviously depends on very fine crystal details.

The Jahn–Teller distortion in ammonium chromous Tutton salt changes slightly with temperature. Alcock *et al.* (1984) also observed the same feature in the copper salt and fitted their results to a simple two-state model in which for each state the Cu—O bond lengths differ. Application of that model here gives a good fit to the six observed bond lengths if we assume an energy of $-450\,(40)\,cm^{-1}$ and Jahn–Teller-distorted bond lengths of 2·053 [Cr—O(9)], 2·078 [Cr—O(7)] and 2·390 Å [Cr—O(8)] for both states. These fitted bond lengths are of same order and have the same relative spacing observed at 5 K for the deuterated copper salt. This gives 18 and 0% occupation of the minority state at 295 and 84 K respectively. We also see the unexpected features of *a* and *b* shrinking on increase in temperature. A simple two-state model may be an oversimplification. Hathaway & Hewat suggested that the basic driving force for the process is connected with the rotational changes of the ammonium ion which they observed. However, in any case, we can conclude that at 84 K the disorder is negligible and will not affect the charge-density analysis.

*Anharmonicity*

The presence of a significant $|\mathbf{k}|^4$ term in the refinement at both temperatures indicates a possible substantial deviation from harmonic ordered-crystal behaviour. However, from this X-ray diffraction experiment alone we cannot exclude the possibility that the effect arises from the deformation electronic density rather than from nuclear motion. A neutron diffraction study to high values of $|\mathbf{k}|$ on a suitable Tutton-salt crystal would define thermal terms very accurately, and thus settle whether we have indeed observed anharmonic effects or only modelled electron density effects in terms of nuclear-motional effects. We plan such an experiment. However, the effect is well enough described for the present that we can continue with a charge-density analysis of more diffuse-valence features.

*Deformation density maps*

The deformation density maps of Figs. 1–3 show peaks at the Cr-atom site and *ca* 0·40 Å from each O atom along the Cr—O vector. The peak at Cr indicates a gain in its 3*d* population over the atomic $3d^4$ configuration. The peak is elongated along the Cr—O(8) vector, and there are holes in the Cr–O(7)–O(9) plane along the metal–oxygen directions. Both these features are explicable in terms of a deficiency of density in the $3d_{x^2-y^2}$ orbital. We thus have evidence that the Jahn–Teller distortion has caused the expected hole in the 3*d* configuration, and that covalence is present.

The peaks on the O atoms are those expected from their lone pairs. The maxima for O(8) and O(9) are on the metal–oxygen bond axis, and for O(7) almost so. The Cr—O—H angles are nearly equal in each water molecule, ensuring the Cr—O vector is almost in the plane perpendicular to that of $OH_2$ and bisecting the H—O—H angles. The metal coordination is optimum for overlap with the water-molecule lone pairs, which are at a maximum in this plane. We also expect these lone pairs to be more extended in this plane than perpendicular to it. Therefore, if we measure the distances perpendicular to the Cr—O vector, through each O atom, from one 0·1 e $Å^{-3}$ contour to another, we should find the in-water plane value to be less than for the out-of-water plane. We see for O(7) to O(9): in-plane 1·25, 1·08 and 1·29, and for out-of-plane 1·54, 1·74 and 1·74 Å. We conclude that we do indeed see that the oxygen pair of lone pairs is extended more perpendicular to the water plane than in the water plane. The lone-pair heights are respectively 0·5, 0·8 and 0·6 e $Å^{-3}$. The O(8) water lone pair is both less extended in space and higher than the other two, suggesting that the O(7) and O(9) water molecules are more covalently bonded than are those corresponding to O(8).

Fig. 4 shows a typical section through the sulfate ion. All other sections, identical in $T_d$, are very similar even in this lower-symmetry crystal and so are not shown. We see a large mid-bond peak of *ca* 0·7 e $Å^{-3}$ in each S—O bond, a lone-pair region on each O atom on the far side of the S—O bond, and three holes *ca* 0·9 Å from the S atom. These holes come from sections through negative regions of tetrahedral symmetry. The negative regions minimize at the opposite tetrahedral corners from the sulfate O atoms, but join, forming, at this radius from S, an almost continuous band, interrupted only by the strongly positive S—O bond area.

The ammonium ion section of Fig. 5 is representative of all such sections and is featureless apart from a peak on the N atom. Because of our use of X-ray-determined hydrogen positions and thermal parameters, any deformation density resulting from bonding would not be seen in these maps.

*Population analysis*

The qualitative discussion above has indicated the presence in the $Cr(OH_2)_6$ unit of a Jahn–Teller distortion of the chromium 3*d* shell and covalent effects

stronger from the O(7) and O(9) water molecules than from that of O(8), but analyses of the relevant populations are required to quantify these effects.

After removing the model valence density from the deformation density maps of Figs. 1–5, the residual density shown in Figs. 6–10 is negligible. The only possibly significant feature in Fig. 6 is a small peak at 0·6 Å from the Cr atom. The refinements R5 and R6 have described virtually all significant information in the experiment, a fact which is also indicated by the goodness of fit, $\chi^2 \simeq 1$. We discuss the tetragonally constrained results of R6 since these are not significantly different from the symmetry unconstrained results of R5 but are simpler to visualize. We must assume that our treatment of thermal motion is adequate to deconvolute a static density from these dynamic density results.

Any population analysis is biased, in the sense that the population parameters are dependent on the model employed. We illustrate this in Table 4, where the charges on the sulfate and ammonium, although not the hexaaquametal, ions, differ depending on the method used to extract the charges from the thermally smeared data. Differences are more marked the more the fragments overlap and interact. In this case both methods of analysis agree in that the charges on the fragments, while still marked, are mostly reduced from the free-ion values. In the case of $Cr(OH_2)_6$, the reduction is from +2 to +1·21 (17) or +1·18 (11); for $SO_4$ from −2 to −1·33 (13) or −1·66 (5); and for $NH_4$ from +1 to +0·74 (16) or +1·07 (3). This reduction, as well as the different values for each method of division, are indicative of the relatively strong hydrogen bonding with accompanying charge transfer from donor to H atom in the Tutton salts.

The hexaaquametal ion charges are more interesting than the sulfate and ammonium fragments. We note the transfer of 0·81 (22) e from the water molecules to the formal $Cr^{2+}$ ion. The water molecules, however, remain essentially neutral, the electron loss to the chromium being balanced by the donation from the sulfate ion to the H atoms by hydrogen bonding. The water molecules differ amongst themselves. The unconstrained refinement shows that the O(7) and O(9) water molecules are similar to each other and different from that of O(8). If we use H-atom positions estimated from neutron diffraction on other ammonium Tutton salts, the O(7) and O(9) water molecules have approximately a 50% greater dipole moment compared with the O(8) case. This increase is entirely due to polarization in the O—H bond. The lone-pair population acts in the opposite direction; the O(8) lone-pair population is greater than for those of O(7) and O(9).

The observations of the previous paragraph agree very well with qualitative results of theoretical calculations (Hermansson, Olovsson & Lunell, 1984). These, and our results, can be interpreted to say that the effect of bonding a set of six arranged water molecules to a metal atom is to polarize the O—H bond, increasing charge behind the O atom, while charge is donated to the metal from the oxygen lone-pair. In addition, theory predicts an increase in density in the mid-bond region resulting from the bond-overlap term. We see a very significant such overlap term [0·15 (2) e] for the O(7) and O(9) but none [0·00 (2) e] for the O(8) water bond. Thus, from the distribution of charge around the water molecules, we conclude that O(7) and O(9) bond much more strongly to the Cr atom than does O(8), and that both the distributions on the water molecules and the differences between them confirm the picture obtained by Hermansson *et al.* from theoretical calculations.

When we turn to the chromium 3*d*- and 4*p*-orbital populations, this conclusion is strengthened. A tetragonally distorted $3d^4$ ion, such as here, would be expected to have a configuration $3d^1_{xy}\ 3d^2_{xz,yz}\ 3d^1_{z^2}\ 3d^0_{x^2-y^2}$. This resembles what is observed in practice; $3d^{1\cdot26(3)}_{xy}\ 3d^{2\cdot04(4)}_{xz,yz}\ 3d^{0\cdot88(4)}_{z^2}\ 3d^{0\cdot28(3)}_{x^2-y^2}$, but with significant differences, which are due to covalence. If we assume that the O(7) and O(9) water molecules $\sigma$ donate charge into the $3d_{x^2-y^2}$ and $3d_{z^2}$ orbitals while O(8) does not participate, we expect both populations to increase, $3d_{x^2-y^2}$ at three times the rate of $3d_{z^2}$ owing to the three times greater overlap of O(7) and O(9) with $3d_{x^2-y^2}$ than with $3d_{z^2}$. We observe an increase of 0·28 (3) in $3d_{x^2-y^2}$ but a decrease in $3d_{z^2}$ of 0·12 (4) e. However, we also notice that, while the $4p_x$ and $4p_y$ populations are negative, that of $4p_z$ is large and positive. It has been inferred from cellular ligand-field studies of the spectroscopy in square-planar complexes that in these systems excess electron density accumulates in the vacant coordination site, perhaps by $3d_{z^2}$–$4s$ hybridization (Deeth, Duer & Gerloch, 1987*a*,*b*; Deeth & Gerloch, 1987). Our observations of excess diffuse density at the weakly coordinated sites provide evidence for this supposition. We see strong $\sigma$ donation into the $3d_{x^2-y^2}$ orbital from O(7) and O(9), while the lack of coordination from O(8) not only causes the $3d_{z^2}$ population to be low, it even, by hydridization with the diffuse $4s/p/d$ orbitals, reduces the population below 1·00 and gives a large diffuse population along the Cr—O(8) vector. We note that this excess '$4p_z$' (or possibly expanded $3d_{z^2}$) population is closer to the metal than the mid-bond overlap region and thus distinguishable from it experimentally.

We also expect some $\pi$-bonding into the $3d_{xy,xz,yz}$ orbitals. These do increase in population, with $3d_{xy}$ at 1·26 (3) significantly larger than 1·00. The interpretation that O(7) and O(9) $\pi$-donate, while O(8) does not, is consistent with this.

## Concluding remarks

The experimental charge density in the present ammonium chromous Tutton salt allows us to make three broad conclusions.

(1) Intermolecular effects are visible in the charge density in, for example, the donation of *ca* 0·5 e from each sulfate to the chromium hexaaqua ion, reducing its charge from +2 to *ca* +1, but these do not perturb the local symmetry of an ion. The charge density of each atom can still be described, to within the accuracy of this experiment, with one minor exception, by functions adapted to its local, nearest-neighbour symmetry. We see no long-range or non-local effects. A consequence of this is that a chemically based model using 3*d* orbitals on chromium and 2*s*–2*p* hybrid and $p_\pi$ orbitals on O atoms can provide a complete model of the deformation density.

(2) We detect covalence in the chromium–water bonding. The water molecule is polarized, with the O—H bond becoming more polar. There is both $\sigma$- and $\pi$-bonding charge transfer into the chromium 3*d* orbitals in comparable amounts, with the $\sigma$ donation coming from the oxygen lone pairs. A mid-bond overlap density is also significant. This pattern of deformation density is just that predicted theoretically by Hermansson *et al.* (1984).

(3) The Jahn–Teller distortion has distinct effects. The chromium 3*d* density is depleted in $3d_{x^2-y^2}$ to give an almost unit hole, as expected from crystal-field theory. The metal density along the long bond changes, the population of the $3d_{z^2}$ orbital decreases slightly while a diffuse $4p_z$-like density increases significantly. Thus as the bond lengthens, and a 'coordination void' is produced, it is to some extent filled with excess electron density.

The authors are indebted to the University of Western Australia Crystallography Centre for access to the diffractometer and to the Australian Research Council for financial support.

### References


ABRAGAM, A. & PRYCE, M. H. L. (1951). *Proc. R. Soc. London Ser. A*, **205**, 35–153.

ALCOCK, N. W., DUGGAN, M., MURRAY, A., TYAGI, S., HATHAWAY, B. J. & HEWAT, A. (1984). *J. Chem. Soc. Dalton Trans.* pp. 7–14.

BROWN, G. M. & CHIDAMBARAM, R. (1969). *Acta Cryst.* B**25**, 676–687.

CLEMENTI, E. & ROETTI, C. (1974). *At. Data Nucl. Data Tables*, **14**, 177–478.

CROMER, D. T. & LIBERMAN, D. (1970). *J. Chem. Phys.* **53**, 1891–1898.

DEETH, R. J., DUER, M. J. & GERLOCH, M. (1987*a*). *Inorg. Chem.* **26**, 2573–2578.

DEETH, R. J., DUER, M. J. & GERLOCH, M. (1987*b*). *Inorg. Chem.* **26**, 2578–2582.

DEETH, R. J., FIGGIS, B. N., FORSYTH, J. B., KUCHARSKI, E. S. & REYNOLDS, P. A. (1989). *Proc. R. Soc. London Ser. A*, **421**, 153–168.

DEETH, R. J. & GERLOCH, M. (1987). *Inorg. Chem.* **26**, 2582–2586.

EARNSHAW, A., LARKWORTHY, L. F., PATEL, K. C. & BEECH, G. (1969). *J. Chem. Soc. A*, pp. 1334–1339.

FENDER, B. E. F., FIGGIS, B. N. & FORSYTH, J. B. (1986*a*). *Aust. J. Chem.* **39**, 1023–1028.

FENDER, B. E. F., FIGGIS, B. N. & FORSYTH, J. B. (1986*b*). *Proc. R. Soc. London Ser. A*, **404**, 139–145.

FENDER, B. E. F., FIGGIS, B. N., FORSYTH, J. B., REYNOLDS, P. A. & STEVENS, E. (1986). *Proc. R. Soc. London. Ser. A*, **404**, 127–138.

FIGGIS, B. N., FORSYTH, J. B., KUCHARSKI, E. S., REYNOLDS, P. A. & TASSET, F. (1989). *Proc. R. Soc. London Ser. A*, **428**, 113–124.

FIGGIS, B. N., KUCHARSKI, E. S. & REYNOLDS, P. A. (1989). *Acta Cryst.* B**45**, 240–247.

FIGGIS, B. N., KUCHARSKI, E. S., REYNOLDS, P. A. & TASSET, F. (1989). *Acta Cryst.* C**45**, 942–944.

FIGGIS, B. N. & REYNOLDS, P. A. (1985). *Inorg. Chem.* **24**, 1864–1873.

FIGGIS, B. N., REYNOLDS, P. A. & WHITE, A. H. (1987). *J. Chem. Soc. Dalton Trans.* pp. 1737–1745.

FIGGIS, B. N., REYNOLDS, P. A. & WILLIAMS, G. A. (1980). *J. Chem. Soc. Dalton Trans.* pp. 2339–2347.

FIGGIS, B. N., REYNOLDS, P. A. & WRIGHT, S. (1983). *J. Am. Chem. Soc.* **105**, 434–440.

GRIMES, N. W., KAY, H. F. & WEBB, M. W. (1963). *Acta Cryst.* **16**, 823–829.

HALL, S. R. & STEWART, J. M. (1989). Editors. *XTAL*2.6 *Users Manual.* Univs. of Western Australia, Australia, and Maryland, USA.

HATHAWAY, B. J. & HEWAT, A. W. (1984). *J. Solid State Chem.* **51**, 364–375.

HERMANSSON, K., OLOVSSON, I. & LUNELL, S. (1984). *Theor. Chim. Acta*, **64**, 256–276.

HIRSHFELD, F. (1977). *Theor. Chim. Acta*, **44**, 129–138.

IWATA, M. (1977). *Acta Cryst.* B**33**, 59–69.

MASLEN, E. N., RIDOUT, S. C. & WATSON, K. J. (1988). *Acta Cryst.* B**44**, 96–101.

MASLEN, E. N., RIDOUT, S. C., WATSON, K. J. & MOORE, F. H. (1988). *Acta Cryst.* C**44**, 412–415.

MASLEN, E. N., WATSON, K. J. & MOORE, F. H. (1988). *Acta Cryst.* B**44**, 102–107.

MONTGOMERY, H., CHASTAIN, R. V. & LINGAFELTER, E. C. (1966). *Acta Cryst.* **20**, 731–733.

MONTGOMERY, H., CHASTAIN, R. V., NATT, J. J., WITKOWSKA, A. M. & LINGAFELTER, E. C. (1967). *Acta Cryst.* **22**, 775–780.

MONTGOMERY, H. & LINGAFELTER, E. C. (1964*a*). *Acta Cryst.* **17**, 1295–1299.

MONTGOMERY, H. & LINGAFELTER, E. C. (1964*b*). *Acta Cryst.* **17**, 1478–1479.

MONTGOMERY, H. & LINGAFELTER, E. C. (1966). *Acta Cryst.* **20**, 659–662.

REYNOLDS, P. A. & FIGGIS, B. N. (1989). *Aust. J. Chem.* **42**, 1831–1838.

RILEY, M. J., HITCHMAN, M. A. & MOHAMMED, A. W. (1987). *J. Chem. Phys.* **87**, 3766–3778.

STEWART, J. M., DAVIDSON, E. R. & SIMPSON, W. T. (1965). *J. Chem. Phys.* **87**, 3175–3187.

STEWART, R. F. (1973). *Acta Cryst.* A**29**, 602–605.

TREUSHNIKOV, E. N., KUSKOV, V. E., SOBOLEVA, L. V. & BELOV, N. V. (1978). *Sov. Phys. Crystallogr.* **23**, 14–19.

VAALSTA, T. P. & MASLEN, E. N. (1987). *Acta Cryst.* B**43**, 448–454.

WEBB, M. W., KAY, H. F. & GRIMES, N. W. (1965). *Acta Cryst.* **18**, 740–742.